Experimental Measurement of the Second-Order Coherence of Supercontinuum

Mikko Närhi,[1,*] Jari Turunen,[2] Ari T. Friberg,[2] and Goëry Genty[1]
[1]Department of Physics, Tampere University of Technology, P.O. Box 527, FI-33101 Tampere, Finland
[2]Institute of Photonics, University of Eastern Finland, P.O. Box 111, FI-80101 Joensuu, Finland
(Received 22 September 2015; published 13 June 2016)

We measure experimentally the second-order coherence properties of supercontinuum generated in a photonic crystal fiber. Our approach is based on measuring separately the quasicoherent and quasistationary contributions to the cross-spectral density and mutual coherence functions using a combination of interferometric and nonlinear gating techniques. This allows us to introduce two-dimensional coherence spectrograms which provide a direct characterization and convenient visualization of the spectrotemporal coherence properties. The measured second-order coherence functions are in very good agreement with numerical simulations based on the generalized nonlinear Schrödinger equation. Our results pave the way towards the full experimental characterization of supercontinuum coherence properties. More generally, they provide a generic approach for the complete experimental measurement of the coherence of broadband sources.

DOI: 10.1103/PhysRevLett.116.243901

The physics of supercontinuum (SC) generation in optical fibers has been extensively studied in the past decade [1]. While the physics is now well understood, supercontinuum sources are finding an increasing number of applications ranging from frequency combs and confocal microscopy to optical coherence tomography or hyperspectral imaging. In principle, any powerful laser source can be used to create a SC. Yet, only SC spectra generated from femtosecond pump pulses possess the high phase stability and coherence required for applications in frequency metrology. Unstable incoherent SC spectra, on the other hand, are most suitable for applications where time-averaged measurements are important, as, e.g., in spectroscopy or imaging. Coherence then appears naturally as a critical parameter of SC light sources [2–6].

The spectral degree of "first-order" coherence characterizing the shot-to-shot phase stability at single frequencies [7] has now become the norm to evaluate the spectral coherence of SC. It can be measured using a polychromatic delayed Michelson interferometer (PDMI), where the visibility of the spectral interference fringes produced by two consecutive SC pulses directly corresponds to the coherence degree [8]. However, it was recently shown that this measure of spectral coherence gives only partial information, and that the two-time and two-frequency correlation functions of second-order coherence theory of nonstationary light provide a complete (up to second order in field variable) description of the temporal and spectral coherence of SC light [9,10]. This is because, unlike the first-order degree of coherence, the second-order cross-spectral density (CSD) and mutual coherence function (MCF) measure the correlation between two different frequencies and instants of time, respectively.

The experimental characterization of these second-order coherence functions requires the measurement of single-shot SC amplitude and phase. This is generally not possible due to current electronic limitations and, up to now, only time-integrated measurements corresponding to first-order degree of coherence have been successfully reported [6,11]. Here, using a combination of interferometry and cross-correlation frequency-resolved optical gating (XFROG) [12], we measure experimentally the second-order coherence functions of SC both in the time and frequency domains [10]. This allows us to access the true coherence time and coherence bandwidth of SC. The measurement procedure also enables us to generate the coherence spectrogram corresponding to the mean electric field, which directly links the spectral and temporal coherence properties. We further compare our experimental results with numerical simulations and find good agreement in all the cases investigated. Our results open the route towards modeling and optimizing SC-based optical systems where only the propagation of the second-order coherence functions is required to evaluate the system performance [13–15]. More generally, our experiments provide means to measure the complete coherence characteristics of broadband light sources, with access to the mean electric field, using only time-averaged measurements.

For nonstationary sources the second-order coherence properties are specified by the two-time MCF and two-frequency CSD functions. The normalized MCF and CSD expressed in average $(\bar{t},\ \bar{\omega})$ and difference $(\Delta t,\ \Delta\omega)$ coordinates are defined as

$$\gamma(\bar{t},\Delta t)=\frac{\langle E^*(\bar{t}-\Delta t/2)E(\bar{t}+\Delta t/2)\rangle}{\sqrt{I(\bar{t}-\Delta t/2)I(\bar{t}+\Delta t/2)}}, \qquad (1)$$

$$\mu(\bar{\omega},\Delta\omega)=\frac{\langle\tilde{E}^{*}(\bar{\omega}-\Delta\omega/2)\tilde{E}(\bar{\omega}+\Delta\omega/2)\rangle}{\sqrt{S(\bar{\omega}-\Delta\omega/2)S(\bar{\omega}+\Delta\omega/2)}}, \quad (2)$$

where the angle brackets represent ensemble average over multiple SC electric field realizations $E(t)$ and the asterisk stands for the complex conjugate. $\tilde{E}(\omega)$ is the complex spectral representation of the electric field $E(t)$ obtained by Fourier transform. $I(t)$ and $S(\omega)$ are the mean temporal intensity and spectrum, respectively. These functions are bounded between zero and unity, the latter signifying complete correlation between frequencies and zero corresponding to no correlation. Note that Eqs. (1) and (2) do not form a two-dimensional Fourier transform pair, unlike their non-normalized form [13].

Recent numerical studies have shown that the MCF and CSD can approximately be separated into two distinct contributions—a quasicoherent square within which the spectral or temporal components are fully correlated and a quasistationary line representing the uncorrelated, noise-driven SC components [9,10]:

$$\gamma(\bar{t},\Delta t)\approx\gamma_c(\bar{t},\Delta t)+\gamma_q(\Delta t), \quad (3)$$

$$\mu(\bar{\omega},\Delta\omega)\approx\mu_c(\bar{\omega},\Delta\omega)+\mu_q(\Delta\omega), \quad (4)$$

where the subscripts c and q correspond to the coherent square and quasistationary line, respectively. From a physical point of view, the coherent square and quasistationary line represent the spectral or temporal interval within which the SC exhibits temporal and spectral coherence properties similar to those of a laser and a classical incoherent source, respectively. Because of the bandwidth limitations of currently available photodetectors, it is generally not possible to measure the shot-to-shot complex electric field of SC light and thus access directly the second-order correlation functions. Taking advantage of the separation of the coherence functions into a coherent and a quasistationary part, an indirect approach was suggested in Ref. [10]. Specifically, it was shown that the coherent contribution essentially corresponds to a cross product of one-argument first-order degrees of spectral coherence:

$$\mu_c(\bar{\omega},\Delta\omega)=\frac{\tilde{E}_c{}^{*}(\bar{\omega}-\Delta\omega/2)\tilde{E}_c(\bar{\omega}+\Delta\omega/2)}{\sqrt{S(\bar{\omega}-\Delta\omega/2)S(\bar{\omega}+\Delta\omega/2)}}$$
$$\approx\sqrt{|g_{12}^{(1)}(\bar{\omega})||g_{12}^{(1)}(\Delta\omega)|}, \quad (5)$$

where $g_{12}^{(1)}(\omega)=\langle\tilde{E}_i^{*}(\omega)\tilde{E}_j(\omega)\rangle_{i\neq j}/\langle|\tilde{E}(\omega)|^2\rangle$ is the first-order degree of spectral coherence [7]. Its absolute value can be obtained from the visibility of the spectral interference fringes measured from a PDMI.

The quasistationary part of the CSD, $\mu_q(\Delta\omega)$, can be inferred from the Fourier transform of the quasistationary intensity $I_q(t)$:

$$\mu_q(\Delta\omega)=\frac{1}{E_0}\int_{-\infty}^{\infty}I_q(\bar{t})\exp(i\Delta\omega\bar{t})d\bar{t}, \quad (6)$$

where $E_0=(2\pi)^{-1}\int_{-\infty}^{\infty}I(t)dt$ is the total pulse energy. Measuring the XFROG trace allows us to access directly the quasistationary intensity $I_q(t)$ by filtering out the spectral components where interference fringes are observed in the PDMI and integrating over the filtered spectrum. Similarly, the coherent and quasistationary contributions of the MCF can be obtained from the first-order degree of spectral coherence and XFROG with appropriate filtering [10]. Hence, by measuring simultaneously the interference fringes in a PDMI and the corresponding XFROG trace, one can retrieve the experimental second-order coherence functions of SC light. Of course, it is important to bear in mind that the XFROG trace is the convolution of the actual SC complex field with the XFROG gate pulse, and a gate pulse with duration close to 100 fs generally yields a good compromise between temporal and spectral resolution. Note also that the functions are, in general, complex valued, and that only the absolute values are obtained by the procedure described above. However, the non-normalized CSD and MCF form a Fourier transform pair, which in principle allows for an approximate phase retrieval.

A schematic of our experimental arrangement is shown in Fig. 1. We used a Ti:sapphire laser (Spectra Physics Tsunami) at 785 nm producing pulses of 72 fs duration (FWHM) at 80 MHz repetition rate. An isolator placed after the laser to avoid any backreflection stretched the pulse duration to 290 fs. The pulses were then injected into a 69 cm polarization-maintaining photonic crystal fiber (NL-PM-750 from NKT Photonics). A polarizer and half-wave plate combination was applied to vary the input power. A pellicle beam splitter allowed us to extract a small fraction of the 72 fs pulses as the XFROG gate. A rapidly rotated

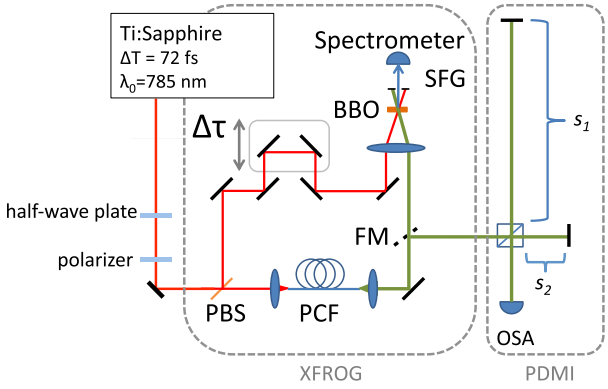

FIG. 1. Experimental setup. PBS, pellicle beam splitter; FM, flip mirror; BBO, beta-barium-borate nonlinear crystal used for SFG (sum-frequency generation); PCF, photonic crystal fiber; $\Delta\tau$, variable delay on a motorized stage; OI, optical isolator; OSA, optical spectrum analyzer.

1 mm thick beta-barium borate crystal was used in the XFROG to allow phase matching across the full SC bandwidth [16]. The grating spectrometer (Avantes AvaSpec-2048L) with adjustable integration time ensured that all the phase-matched signals were recorded during the crystal rotation. Second-harmonic generation FROG was performed to characterize the gate and input pulses.

The SC spectra generated for three different input peak powers are shown in Fig. 2 as black lines (top panels). For an input peak power of $P_p = 70$ W [Fig. 2(a)] the SC spectrum spans approximately 200 nm with a fine structure visible across the entire bandwidth. Such fine structure typically indicates high spectral degree of coherence, as confirmed by the measurement from the PDMI also shown in the figure (red solid lines). Indeed, we can see how the measured first-order coherence function $|g_{12}^{(1)}|$ shows uniform behavior over the full spectrum with values exceeding 0.9.

When the peak power is raised to 360 W [Fig. 2(c)], the SC bandwidth increases to 350 nm and some fine structure can still be observed but with a lower contrast than in the low peak-power case. The decrease in the spectral fine-structure contrast indicates a loss of coherence, as confirmed by the measured first-order spectral coherence function which drops below 0.5 at nearly every wavelength. For an input peak power of 820 W [Fig. 2(e)], the spectrum spans an octave from 550 to 1150 nm (−20 dB bandwidth) and the fine spectral structure is completely washed out, indicating large shot-to-shot fluctuations. The spectral coherence function is nearly 0 across the entire spectrum except around the pump where residual coherence can be observed. For comparison, we ran a series of 500 numerical simulations using the generalized nonlinear Schrödinger equation. We employed the fiber dispersion and nonlinear coefficients provided by the manufacturer, the experimentally measured Raman gain of silica, and a one photon per mode model for the noise implementation. The peak power was increased by 30% in the simulations as compared to the experiments to account for losses in the experimentally measured power. The simulation grid contained 2^{14} points spanning a range of 22 ps and resulting in a temporal and spectral resolution of 1 fs and 50 GHz, respectively.

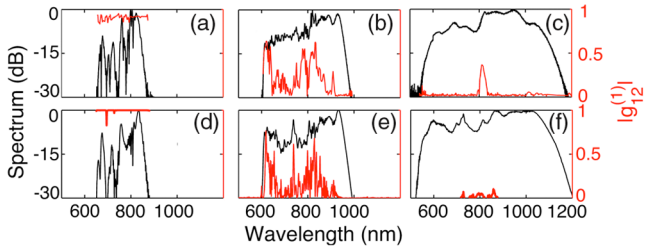

FIG. 2. Experimentally recorded SC spectra (black lines) and measured $|g_{12}^{(1)}|$ (red lines) for peak powers of (a) $P_p = 70$ W, (b) $P_p = 360$ W, and (c) $P_p = 820$ W. Corresponding numerical simulations are shown in (d)–(f).

The results are also shown in Fig. 2 (bottom panels). For all three cases, we see a very good agreement between the measured and simulated spectra on one hand and the spectral coherence functions on the other hand. We do notice small discrepancies, which we attribute to the uncertainty on the dispersion profile of the fiber.

We next proceed to the experimental reconstruction of the second-order coherence functions as described above. The experimentally reconstructed CSDs are plotted in the top panels of Fig. 3. For comparison, the numerically simulated CSDs from the ensemble of realizations are also shown (bottom panels). We observe again a very good agreement between experiments and simulations and, in particular, we see how the coherent square reduces and the quasistationary line becomes more pronounced as the peak power is increased.

The results can be explained in light of the SC dynamics. At a peak power of 70 W [Fig. 3(a)] the soliton order $N = 6$, such that the soliton fission process that leads to the broadband SC is seeded by the pump spectral components. The process is highly deterministic between the input and output, leading to nearly perfect coherence in the generated SC. In this case the CSD is simply a coherent square where spectral components are perfectly correlated. When the peak power is increased to 360 W [Fig. 3(c)], the soliton order $N = 15$, such that competition exists between deterministic soliton fission and stochastic modulation instability seeded from noise outside the pump spectral components which degrades the spectral correlations. The degradation is largest at the long wavelength edge where the peak power and the duration of the ejected solitons from the fission process fluctuate from shot to shot, translating into significant spectral jitter through the soliton self-frequency shift. On the other hand, the dispersive waves, which are emitted at the early stage of the fission

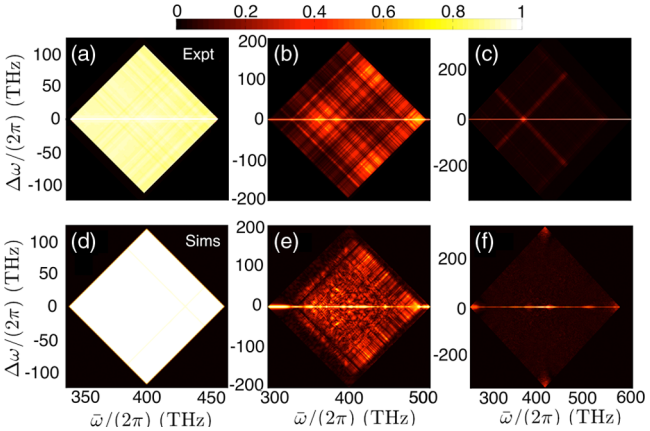

FIG. 3. Experimental (top) and simulated (bottom) CSDs for (a), (d) $P_p = 70$ W, (b), (e) $P_p = 360$ W, and (c), (f) $P_p = 820$ W. The numerical results were two-dimensionally convolved with a Gaussian (2 nm width) function to produce results with resolution comparable to that of our experiments.

process, are less affected by spectral jitter, especially because the fiber is too short for the long wavelength solitons to interact significantly with the dispersive waves through cross-phase modulation. The area of residual coherence in the central part of the spectrum corresponds to pump remain and solitons with low peak power having experienced a small frequency shift. It is interesting to note that the width of the quasistationary line of the simulated CSD is not exactly constant across the full spectrum unlike in the experimentally reconstructed CSD where the approach automatically leads to a constant width. This difference originates from the fact that the separation into a coherent and stationary part is least accurate in the partially coherent case [10]. The experimentally measured coherence bandwidth was found to be 0.9 THz, whereas in the simulations its average value integrated across the full spectrum is about 2.5 THz. For a peak power of 820 W [Fig. 3(e)], the initial stage of SC generation is triggered by noise-seeded modulation instability leading to stochastic variations at the fiber output and no correlations among the spectral components except around the pump remain due to residual coherent self-phase modulation in the initial stage. The CSD in this case thus reduces to a quasistationary line with a coherence bandwidth of 0.55 THz, in good agreement with the numerically simulated result of 1.2 THz.

The experimentally reconstructed and simulated MCFs are shown in Fig. 4. In general, the MCF reconstruction is less accurate than that of the CSD, when compared with the numerical simulations. This is due to the fact that the coherent part of the MCF is measured indirectly unlike for the CSD. Specifically, one frequency may generally consist of contributions from two different (but nearby) time instants of the SC, and filtering in the spectral domain

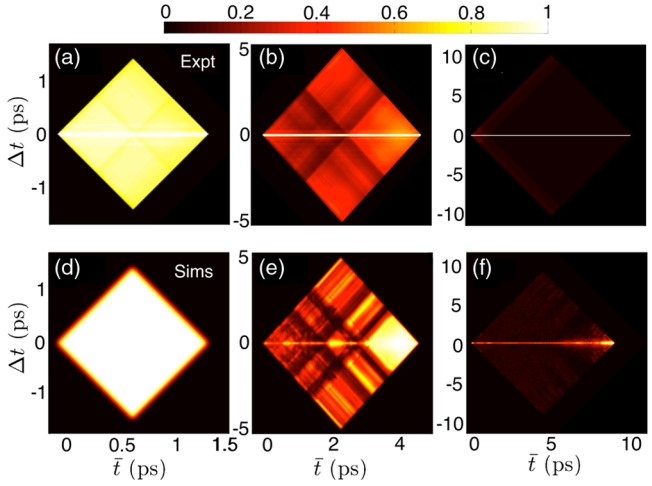

FIG. 4. Experimental (top panels) and simulated (bottom panels) MCFs for (a), (d) $P_p = 70$ W, (b), (e) $P_p = 360$ W, and (c), (f) $P_p = 820$ W. The numerical results were two-dimensionally convolved with a Gaussian (72 fs width) function to produce results with resolution comparable to that of our experiments.

can cause two time instants to have the same degree of coherence even though they actually may be somewhat different. At a low peak power [Fig. 4(a)], the MCF consists of only a coherent square with quasiperfect time correlations, consistent with the CSD and similar to what would be observed for a coherent broadband laser source. In the partially coherent case [Fig. 4(c)], the quasistationary line appears with an average coherence time of 6 fs. The coherent square is degraded, mostly around the solitonic components, while the time correlations are larger for the intensity of the dispersive wave components, as observed in the CSD measurements. Finally, for a large peak power [Fig. 4(e)], the MCF reduces to a quasistationary line with coherence time of 3 fs, corresponding precisely to the inverse spectral bandwidth of the SC in this case and indicating that the SC essentially behaves as a thermal source in terms of temporal coherence (the spatial coherence is still high).

The second-order coherence functions allow us to characterize, separately in the time and spectral domains, the coherence properties of a broadband light source. We illustrate in Fig. 5 how additional information can be obtained using the spectrogram of the mean electric field $\langle E(t) \rangle$. Whereas the mean spectrogram provides the average phase relationship between the spectral and temporal components, it does not furnish any quantitative information on their relative coherence. The spectrotemporal coherence, on the other hand, is fully described by the spectrogram of the mean field, which favors the coherent parts of the pulse due to constructive interference and conversely attenuates the incoherent parts. This quantity is not directly accessible experimentally; however, we demonstrate in Fig. 5 that by filtering the XFROG spectrogram with the spectral coherence function, one can generate "coherence" spectrograms, approximately corresponding to the spectrotemporal representation of the mean electric field and providing a clear spectrotemporal picture of the

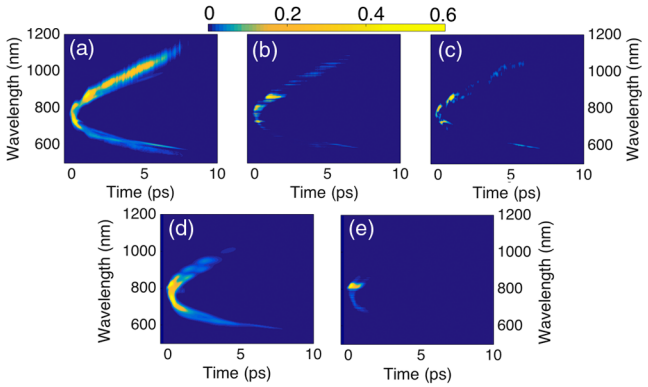

FIG. 5. Top row: Numerical simulations. (a) Average spectrogram, (b) coherence spectrogram obtained by filtering, and (c) spectrogram of the mean complex electric field. Bottom row: Experimental results. (d) Average spectrogram and (e) coherence spectrogram.

SC pulse coherence. We focus on the $P_p = 820$ W case, but the results can readily be extended to the other cases. One can see from the numerical simulations presented in Figs. 5(a)–5(c) how the trace obtained from the filtered spectrogram follows closely the spectrogram of the mean field, allowing us to unambiguously identify the spectrotemporal components of the SC that are carriers of high or low coherence. For comparison, the experimentally measured mean spectrogram and the retrieved coherence spectrogram are plotted in Figs. 5(d) and 5(e), respectively, showing good agreement with the numerical simulations. The coherence spectrogram conveniently reveals the spectrotemporal structure of the mean electric field corresponding to the distribution of the electric field that is coherent on average and thus can be recompressed or postprocessed. This is in contrast with a simple FROG or XFROG trace which does not provide information on the mean electric field.

In conclusion, we have measured the second-order coherence functions of SC light, which are the only quantities required to evaluate the performance of a SC source in an optical system. Our results permit us to measure the true coherence time and coherence bandwidth of SC and provide a generic experimental method for the full characterization of the coherence of nonstationary broadband sources. Finally, our experiments enable us to obtain a clear spectrotemporal picture of the coherence of broadband nonstationary light sources through the concept of a coherence spectrogram that approximately corresponds to the spectrogram of the mean electric field.

This work was supported by the Academy of Finland (Projects No. 267576 and No. 268480).

*Corresponding author.
mikko.narhi@tut.fi

[1] J. M. Dudley, G. Genty, and S. Coen, Rev. Mod. Phys. **78**, 1135 (2006).
[2] T. Udem, R. Holzwarth, and T. W. Hänsch, Nature (London) **416**, 233 (2002).
[3] N. R. Newbury, Nat. Photonics **5**, 186 (2011).
[4] I. Hartl, X. D. Li, C. Chudoba, R. K. Ghanta, T. H. Ko, J. G. Fujimoto, J. K. Ranka, and R. S. Windeler, Opt. Lett. **26**, 608 (2001).
[5] B. Schenkel, R. Paschotta, and U. Keller, J. Opt. Soc. Am. B **22**, 687 (2005).
[6] I. Zeylikovich, V. Kartazaev, and R. R. Alfano, J. Opt. Soc. Am. B **22**, 1453 (2005).
[7] J. M. Dudley and S. Coen, Opt. Lett. **27**, 1180 (2002).
[8] M. Bellini and T. W. Hänsch, Opt. Lett. **25**, 1049 (2000).
[9] G. Genty, M. Surakka, J. Turunen, and A. T. Friberg, Opt. Lett. **35**, 3057 (2010).
[10] G. Genty, M. Surakka, J. Turunen, and A. T. Friberg, J. Opt. Soc. Am. B **28**, 2301 (2011).
[11] X. Gu, M. Kimmel, A. P. Shreenath, R. Trebino, J. M. Dudley, S. Coen, and R. S. Windeler, Opt. Express **11**, 2697 (2003).
[12] J. Dudley, X. Gu, L. Xu, M. Kimmel, E. Zeek, P. O'Shea, R. Trebino, S. Coen, and R. Windeler, Opt. Express **10**, 1215 (2002).
[13] L. Mandel and E. Wolf, *Optical Coherence and Quantum Optics* (Cambridge University Press, Cambridge, England, 1995).
[14] M. Korhonen, A. T. Friberg, J. Turunen, and G. Genty, J. Opt. Soc. Am. B **30**, 21 (2013).
[15] M. Erkintalo, M. Surakka, J. Turunen, A. T. Friberg, and G. Genty, Opt. Lett. **37**, 169 (2012).
[16] P. O'Shea, M. Kimmel, X. Gu, and R. Trebino, Opt. Express **7**, 342 (2000).